JOURNAL OF GEOPHYSICAL RESEARCH, VOL. 115, D05106, doi:10.1029/2009JD012861, 2010

Precursors of the El Niño/La Niña onset and their interrelationship

Jong-Seong Kug,[1] K.-P. Sooraj,[2] Tim Li,[2] and Fei-Fei Jin[3]

Received 21 July 2009; revised 20 December 2009; accepted 27 January 2010; published 10 March 2010.

[1] In this study, the equatorial sea level, western Pacific zonal wind, and high-frequency (2~90 day) wind variability are investigated as precursors of the onset of El Niño/La Niña. To a large extent, it is shown that each variable is a good indicator of El Niño–Southern Oscillation (ENSO) onset by exhibiting significant correlation to the ENSO index with 9 month lag. However, it is demonstrated here that the three precursors are remarkably correlated with each other. Based on the statistical analysis, we suggest here that the three precursors are governed by strong coupling processes: (1) scale interaction within the atmosphere between the low-frequency (LF, i.e., interannual) and high-frequency (HF, i.e., intraseasonal) winds and (2) positive air-sea coupled feedback among the western Pacific westerly, SST, and zonal mean thermocline. Our observational analysis and statistical prediction experiments suggest that the three precursors are not independent and they reflect the different aspects of the same coupling process during the ENSO onset phase.

Citation: Kug, J.-S., K.-P. Sooraj, T. Li, and F.-F. Jin (2010), Precursors of the El Niño/La Niña onset and their interrelationship, *J. Geophys. Res.*, *115*, D05106, doi:10.1029/2009JD012861.

1. Introduction

[2] There has been significant progress in understanding, modeling, and predicting El Niño and La Niña events. Several theoretical models have been suggested to explain the self-sustained oscillation of ENSO. In particular, the recharge paradigm suggested by *Jin* [1997a] and *Li* [1997] tried to explain the oscillating mechanism of ENSO, inferred from the slow ocean adjustment process via the zonal mean heat content exchanges between the equatorial and off-equatorial regions. Many observational, intermediate model and coupled GCM studies have supported this hypothesis [*Meinen and McPhaden*, 2000, 2001; *Perigaud et al.*, 2000; *Cassou and Perigaud*, 2000; *Yu and Mechoso*, 2001; *Kug et al.*, 2003]. However, some observational studies have pointed out that the observed ENSO onsets cannot be explained by this hypothesis as successfully as the developing and decaying processes of ENSO [*Kessler and McPhaden*, 1995; *Kessler*, 2002]. For example, *Kessler* [2002] argued that El Niño phenomena are event-like disturbances with respect to a stable basic state, requiring an initiating impulse not contained in the slow ENSO dynamics. They postulate that this initiation may be carried out by other climate variations [e.g., *Vimont et al.*, 2003a, 2003b]. In addition, several studies pointed out that the stochastic atmospheric "noise" is necessary to trigger and stimulate a damped ENSO variability [e.g., *Blanke et al.*, 1997].

[3] Most El Niño prediction models failed to predict the excessive growth of the largest 1997/1998 El Niño when forecasted from the point prior to El Niño onset in early 1997. In contrast, prediction performed from the point after El Niño onset captured its rapid development quite well [*Barnston et al.*, 1999; *Kang and Kug*, 2000] since ENSO phase tends to be locked to the seasonal cycle. Generally, the predictive skills of dynamic and statistical models are degraded during the ENSO onset period [*Clarke and Van Gorder*, 2003]. This is also related to the so-called spring predictability barrier. Therefore, predicting the El Niño onset is a challenging problem. If we can predict the El Niño onset correctly, it will be possible to predict the tropical Pacific SST up to 18–24 months lead time, because the models have greater predictive skill for the developing and decaying periods of ENSO [e.g., *Luo et al.*, 2008].

[4] In order to predict the onset of El Niño and La Niña, it is important to identify low-frequency (i.e., interannual, hereafter LF) and higher-frequency (HF) precursors. Previous studies have suggested several possible precursors: the zonal mean heat content [*Zebiak and Cane*, 1987; *Jin*, 1997a, 1997b; *Li*, 1997; *Clarke and Van Gorder*, 2003] or warm water volume [*Meinen and McPhaden*, 2000]; HF atmospheric variability such as the Madden Julian Oscillation (MJO) and westerly wind events (WWEs) [*McPhaden*, 1999; *Curtis et al.*, 2004; *Kug et al.*, 2008a]; LF equatorial Western Pacific (WP) winds resulted from midlatitude [*Vimont et al.*, 2001, 2003a, 2003b] and Indian Ocean [*Kug et al.*, 2005; *Clarke and Van Gorder*, 2003] variabilities. However, so far, it is not clear how these precursors are related to each other in leading the El Niño onset. Motivated by this question, in this study we will show their interrela-

[1]Korea Ocean Research and Development Institute, Ansan, Korea.
[2]International Pacific Research Center, SOEST, University of Hawai'i at Mānoa, Honolulu, Hawaii, USA.
[3]Department of Meteorology, SOEST, University of Hawai'i at Mānoa, Honolulu, Hawaii, USA.

0148-0227/10/2009JD012861$09.00

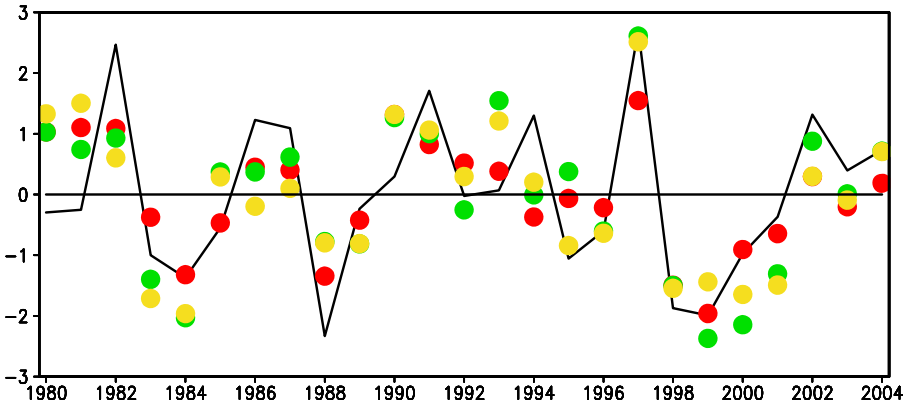

Figure 1. Time series of the normalized NINO3.4 SST (black line) index during NDJ and normalized ZH (red circles), WPU (green circles), and HFU (orange circles) indices during FMA. See the text for more details.

tionship and suggest possible coupling processes among the HF and LF precursors.

2. Data

[5] The data used in this study are monthly means of SST, precipitation, sea level and 925 hPa zonal wind, and daily 925 hPa zonal wind for the period of 1980–2005. The monthly mean SST data are from the improved extended reconstructed sea surface temperature version 2 (ERSST.v2) data set [*Smith and Reynolds*, 2004] created by the National Climate Data Center (NCDC); this data analysis uses monthly and 2° spatial superobservations, which are defined as individual observations averaged onto a 2° grid. The Climate Prediction Center Merged Analysis of Precipitation (CMAP) data were used. The precipitation data were produced by merging rain gauge data, five types of satellite estimates, and a numerical model prediction [*Xie and Arkin*, 1997]. The sea level data utilized are the monthly means of the GODAS product [*Behringer and Xue*, 2004]. The data are available at 1/3° × 1/3° resolution in the tropics.

[6] The monthly and daily wind data are taken from the National Center for Environmental Prediction/National Center for Atmospheric Research (NCEP/NCAR) [*Kalnay et al.*, 1996]. Daily anomalies are calculated after removing the climatologic annual cycle, which is obtained by averaging the all the daily data on the same calendar dates. A 2~90 day band-pass filter (Lanczos filter using 45 weights [*Duchon*, 1979]) is applied to the daily wind anomalies, in order to investigate HF atmospheric variability associated with ENSO. Hereafter, the variability of the filtered wind is referred to as HF variability for simplicity. In this study, we only focus on HF atmospheric variability associated with ENSO. The variance of the filtered wind is calculated for a 3 month moving window.

3. Precursors of El Niño and La Niña Onsets

[7] We initially examine the three possible precursors of El Niño and La Niña onsets, the zonal mean equatorial sea level, the LF WP wind, and the HF wind variability. For easy comparison, the following three precursor indices are defined: (1) ZH index defined as the sea level height anomaly averaged over 150°E–110°W and 5°S–5°N, (2) WPU index defined as the LF zonal wind anomaly averaged over 130°E–170°E, 5°S–5°N, and (3) HFU index defined as the variance of the 2–90 day filtered zonal wind averaged over 130°W–170°W, 5°S–5°N. The averaging area for the HFU index is slightly extended to the east from that for the WPU because the HF variability is closely related to not only vertical shear of LF zonal wind but also zonal gradient of LF zonal wind [*Seiki and Takayabu*, 2007b; *Kug et al.*, 2009a; *Sooraj et al.*, 2009]. Note that the slight change of the definition area does not affect our conclusion. Since El Niño/La Niña has a strong phase-locking feature, the precursors are taken from February to April (FMA), 9 months prior to the typical ENSO peak phase. Sensitivity analyses have been performed with the precursors taken from January to March (JFM) and from March to May (MAM) and the major conclusion also does not change. Here the ENSO peak phase is defined by NINO3.4 SST averaged from November through the following January (NDJ).

[8] Figure 1 shows the time series of the three precursors during the ENSO onset period (FMA), along with the time series of NDJ NINO3.4 SST. Each index is normalized for easy comparison. Note that these three precursor indices lead the NINO3.4 SST by approximately 9 months. In spite of the 9 month lag, the three indices are in general in phase with the NINO3.4 SST, indicating that most El Niño (La Niña) events follow positive (negative) precursor signals, except for the weak 1994 El Niño event. The correlations of the seasonally averaged FMA ZH, WPU and HFU with respect to the NDJ NINO3.4 SST are 0.73, 0.72 and 0.60, respectively, exceeding a 99% confidence level. This indicates that the three indices are good precursors and predictors of the El Niño/La Niña onset, respectively. Note that the autocorrelation between FMA and NDJ NINO3.4 SSTs is 0.1, clearly showing that the precursors beat the persistence.

[9] It is interesting that the three precursors are closely related to each other, regardless of the occurrence of ENSO events. For example, for the years 1980, 1981, 1990, and 1994 the precursors are not matched with the NDJ NINO3.4 SST, but they exhibit similar values to each other, implying that there is a coupled process to govern the precursors

Table 1. Correlation Coefficients Between Indices[a]

	CPSST (FMA)	WPU (FMA)	HFU (FMA)	ZH (FMA)	NINO34 (NDJ)
CPSST	1	**0.80**	0.63	0.68	0.49
WPU		1	**0.89**	**0.83**	**0.72**
HFU			1	**0.83**	0.60
ZH				1	**0.73**

[a]The ZH index is sea level area-averaged over 150°E–110°W and 5°S–5°N; WPU index is U925 wind area-averaged over 130°E–170°E, 5°S–5°N; HFU index is variance of the filtered zonal wind averaged over 130°W–170°W, 5°S–5°N; and CPSST is defined by area-averaging SST over 160°E–180°E, and 5°S–5°N. Boldface emphasizes values greater than 0.7 but less than 1. FMA, February-March-April; NDJ, November-December-January.

beyond the so-called ENSO coupled system such as the Bjerknes feedback. Table 1 summarize the cross correlation between the precursors. In order to investigate air-sea processes associated with the ENSO onset, a central Pacific SST index (CPSST) is additionally defined by spatially averaging SST over 160°E–180°E and 5°S–5°N. The CPSST is significantly correlated to all three precursors. In particular, the correlation between the CPSST and the WPU is highest (0.8). It can be explained that a positive SST anomaly over the central Pacific induces low-level westerlies over the western Pacific and then the anomalous westerlies further enhance the SST anomaly via a deepening thermocline and eastward surface ocean currents. This indicates that a strong air-sea coupling process is evolved even during the onset stage of El Niño and La Niña.

[10] It is remarkable that the WPU is also highly correlated with the HFU and ZH; the correlation coefficients are 0.89 and 0.83, respectively. This high correlation indicates that the LF westerly (easterly) wind anomaly over the western Pacific is closely related to enhanced (suppressed) HF activity and equatorial recharge (discharge) of the heat content. Possible mechanisms that link the HF and LF winds and link the WPU and ZH will be discussed later. Overall, the cross-correlation coefficients between the precursors are greater than those with the NINO3.4 SST index during NDJ, implying that they have a close relationship even in the absence of ENSO.

3.1. Air-Sea Interaction

[11] From Figure 1 and Table 1, it is quite clear that the precursors are closely related to each other, with the cross-correlation coefficients being greater than 0.8. To examine the coherent spatial patterns of the precursors, a linear regression is performed with respect to the WPU. Figure 2 (left) shows these regression patterns during the FMA season. By definition, the regression pattern of zonal winds at 925 hPa shows anomalous westerlies over the equatorial western Pacific from 130°E to the international dateline. It is noted that significant easterly anomalies appear at 20°N. As a result, anomalous cyclonic flows appear over the western north Pacific. The cyclonic flows may be related to the previous La Niña state and the resultant local warm SST [*Weisberg and Wang*, 1997a, 1997b; *Wang et al.*, 2000, 2001] and the cold Indian Ocean SST [*Watanabe and Jin*, 2003; *Kug et al.*, 2005, 2006a, 2006b; *Kug and Kang*, 2006; *Xie et al.*, 2009]. There are also significant easterlies over the eastern Pacific.

[12] The SST and precipitation anomalies (Figures 2b and 2c) clearly show that these anomalous westerlies are results of a strong air-sea coupled process. As expected, the pattern of the precipitation anomaly is consistent with that of the SST anomaly. Namely, a warmer (colder) SST is linked to more (less) precipitation, in spite of a slight westward shift of the precipitation (Figures 2b and 2c). The anomalous precipitation leads to anomalous low-level wind, so that it is well matched with the LF equatorial zonal wind as shown in Figure 2a. It is noted that the SST pattern bears some similarity to the so-called meridional mode [*Chiang and Vimont*, 2004; *Chang et al.*, 2007].

3.2. Scale Interaction Between HF and LF Variability

[13] Figure 2d shows the pattern of the HF variability during the positive phase of the WPU. The HF wind variability is strengthened over the equatorial western Pacific, indicating strong MJO/WWB activity in the region. Relatively strong HF variability also appears over the north central Pacific (180°W–130°W, 10°N–20°N), while weaker HF variability appears over the equatorial eastern Pacific and north western Pacific. It is interesting to note that the pattern of the HF variability resembles that of the LF zonal wind shown in Figure 2a. This indicates the HF variability is closely related the in situ background low-level zonal wind via vertical and horizontal shear [*Seiki and Takayabu*, 2007a, 2007b; *Kug et al.*, 2009a; *Sooraj et al.*, 2009].

[14] Several observational studies showed that HF variability are modulated by the ENSO cycle [*Eisenman et al.*, 2005 *Hendon et al.*, 2007; *Kug et al.*, 2008a, *Tang and Yu*, 2008]. Furthermore, *Kug et al.* [2009a] found that the changes in HF variability associated with ENSO are more closely related to the LF wind anomalies than to the LF SST anomalies by diagnosing the reanalysis data and several model outputs. They also showed that the relation was clearer particularly over the western and central Pacific. In addition, *Sooraj et al.* [2009] further investigated how the LF wind controls the HF atmospheric variability in an idealized atmospheric general circulation model. They showed that the low-level westerlies give a favorable condition for energetic HF variability due to easterly vertical shear [*Wang and Xie*, 1996] and strong horizontal wind shear [*Seiki and Takayabu*, 2007a, 2007b]. Thus, these studies clearly explain the above high correlation between HFU and WPU.

[15] On the other hand, the HF variability, which is modulated by the LF circulation, may in turn affect the LF flow through a feedback loop. It is well known that the HF zonal wind is highly skewed to the westerly phase in the WP (see Figure 3) where the correlation between LF wind and HF variability is higher. While WWEs are observed frequently, EWEs (Easterly Wind Events) are rarely observed. Also, the magnitude of the HF westerly is stronger than that of the HF easterly. If we take long-term mean for strong westerly and weak easterly, it will be westerly residual. Therefore, it is possible that this asymmetric feature of the HF wind can lead to time-mean westerlies which is reflected in the LF and climatological circulation. The magnitude of this residual westerlies depends on the variance of the HF variability. That is, stronger the HF variance, larger the westerly residual is, and vice versa. Therefore, the LF westerlies obtain more westerly residual through the stronger HF activity. This indicates the nonlinear rectification

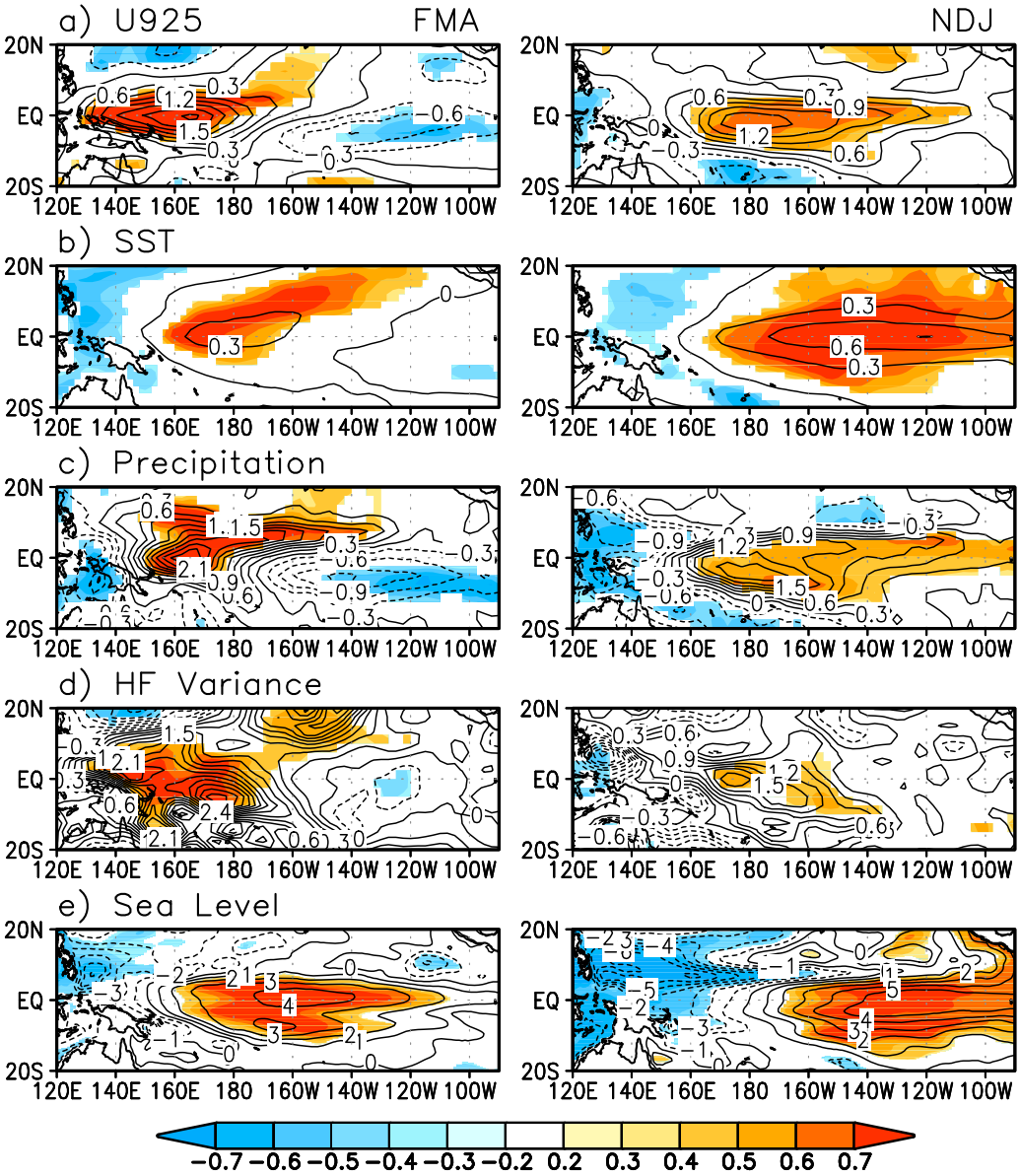

Figure 2. Linear regression (contour) and correlation (shading) of (a) zonal wind at 925 hPa, (b) SST, (c) precipitation, (d) variance of the filtered zonal wind at 925 hPa, and (e) sea level with respect to the FMA WPU index. (left) FMA (0) and (right) ND(0)J(1).

effect of the HF variability can modulate the LF wind variability. In fact, the nonlinear rectification effect has been studied on the tropical interdecadal variation that ENSO asymmetry and its decadal modulation can lead to tropical interdecadal variability [*Rodgers et al.*, 2004; *An*, 2004; *An et al.*, 2005]. This process can be applied to the HF-LF wind interaction. However, our argument on the nonlinear rectification effect of the HF wind is premature, so detail physical processes should be investigated in a further study.

[16] As mentioned, the LF wind modulates the HF variability by providing a favorable background. In addition, the HF variability can also modulate the LF wind variability by the nonlinear rectification effect. This indicates a positive feedback between the HF and LF winds. The high correlation between the HFU and WPU can be explained by this strong two-way positive feedback.

3.3. Role of WP Wind on the Zonal Mean Sea Level Variation

[17] Figure 2e shows a linear regression of the sea level anomaly with respect to the WPU. In accordance with the anomalous westerly pattern over the western Pacific, there are positive sea level anomalies over the central to eastern Pacific and negative anomalies over the northwestern Pacific. Note that this pattern is different from that of the El Niño mature phase, which exhibits an east-west sea-saw pattern as shown in Figure 2e (right). In addition, this pattern is similar to the second EOF mode of the sea level anomaly in the tropical Pacific, known as a precursor signal of ENSO development, while the pattern of El Niño mature phase is similar to the first EOF mode [*Ji et al.*, 2000]. In the conventional ENSO theory, the basin-wide recharge pattern,

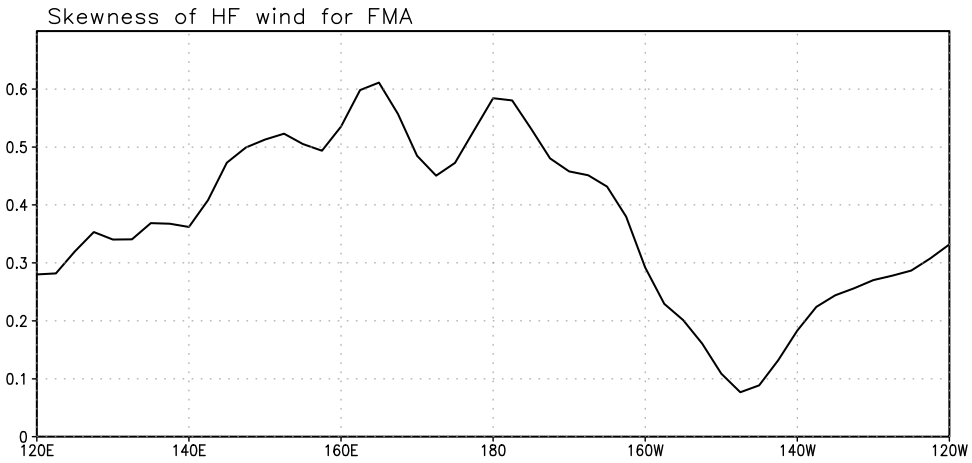

Figure 3. Skewness of the high-frequency (2–90 days) zonal wind along the equator (5°S–5°N) during FMA.

represented by the second EOF mode, is caused by an ocean adjustment process in delayed response to the central Pacific wind anomaly during previous ENSO events [*Jin*, 1997a; *Li*, 1997]. On the other hand, it is suggested here that the sea level pattern is simultaneously related to the WP wind anomaly. For instance, the simultaneous correlation is much higher than the lag correlation with previous ENSO events. This implies that a part of the variability of the second EOF mode is not fully related to the previous ENSO events, but is caused by the HF and LF precursor signals in the WP.

[18] It should be noted that the equatorial sea level maximum in the left panel of Figure 2e is consistent with a nodal point of the equatorial zonal wind. When the sea level anomaly exhibits a strong east-west contrast pattern associated with anomalous westerlies, it leads to strong discharge of heat content (or mass) from the equatorial Pacific to the off-equatorial Pacific by geostrophic meridional transport [*Jin*, 1997a]. In this case, the westerly wind is closely correlated to the tendency of the zonal mean sea level [*Li*, 1997]. Therefore, the zonal mean sea level will be zero when the westerly is at maximum, indicating that their simultaneous correlation is nearly zero. However, this pattern during the ENSO onset phase does not efficiently discharge the equatorial heat content. Since the maximum of sea level anomalies is located over the central Pacific, the anomalous zonal gradient of the sea level anomalies is eastward over the western Pacific and westward over the eastern Pacific. Hence, meridional transport by geostrophic currents is poleward over the western Pacific and equatorward over the eastern Pacific. Thus, they cancel each other out, leading to a relatively weak recharge/discharge. In addition, the western boundary mass transport, which tends to offset the meridional mass transport [*An and Kang*, 2000; *Kug et al.*, 2003], is relatively strong because the action centers of the wind stress and its resultant curl are close to the western boundary. As a result, the equatorial westerlies cannot lead to the discharge of the equatorial heat content any more, when the wind anomaly is located over the western Pacific. Therefore, the LF zonal wind can be simultaneously correlated with the equatorial zonal mean sea level.

[19] To further characterize the lead-lag relationship between westerly wind and zonal mean heat content depending on zonal location of the westerly wind, numerical experiments are performed using the *Zebiak and Cane* [1987] ocean model (hereafter CZ model). This ocean model is forced by a prescribed periodic wind stress field. The formula for the idealized wind stress is expressed as

$$\tau(x,y,t) = \alpha F(x,y)T(t), \tag{1}$$

where $F(x,y)=\{\Psi_0(y/L_y)-\Psi_2(y/L_y)\}\times\left\{\exp\left[-\left(\frac{X-X_0}{L_x}\right)^2\right]-0.2\right\}$ is the spatial function of the wind stress adapted from *An and Wang* [2000] and *Kang and Kug* [2002]; Φ_0 and Φ_2 are the zero-order and the second-order Hermit functions, respectively; X_o specifies the longitudinal position of the maximum wind stress; $L_x = 45^0$ and $L_y = 9^0$; $\alpha = 0.4$ is a scaling coefficient; T(t) is a time-varying sinusoidal function with a time scale of 4 years, sin(t/4yr). The two wind stress patterns are used for the different values of X_o = 140°E and 180°E (hereafter these experiments are denoted as WP Exp and CP Exp, respectively), in order to examine the sensitivity of the zonal mean equatorial thermocline response to the location of the wind stress forcing.

[20] The model is integrated for 100 years in the two experiments. Because the wind stress forcing is purely regular, the response of the ocean model is also mostly regular. Figure 4 shows a lead-lag correlation between wind stress forcing and zonal mean thermocline. When the center of the wind stress is located at 180°E (CP Exp), positive zonal mean thermocline leads positive wind stress forcing by about 9 months. The simultaneous correlation is almost zero. This relation is quite consistent with that of the recharge oscillator [*Jin*, 1997a, 1997b]. On the other hand, the evolution of the zonal mean thermocline is quite different when the wind stress is moved to the west. When the center of the wind stress is located at 140°E (WP Exp), the positive wind stress slightly leads the positive zonal mean thermocline depth, which is quite different response from the conventional ENSO theories. Thus, the simultaneous correlation between wind and zonal mean thermocline depth is high. This result clearly demonstrates that the relation between the equatorial wind and zonal mean thermocline depth highly depends on the zonal location of wind forcing. This process may explain the high correlation between the

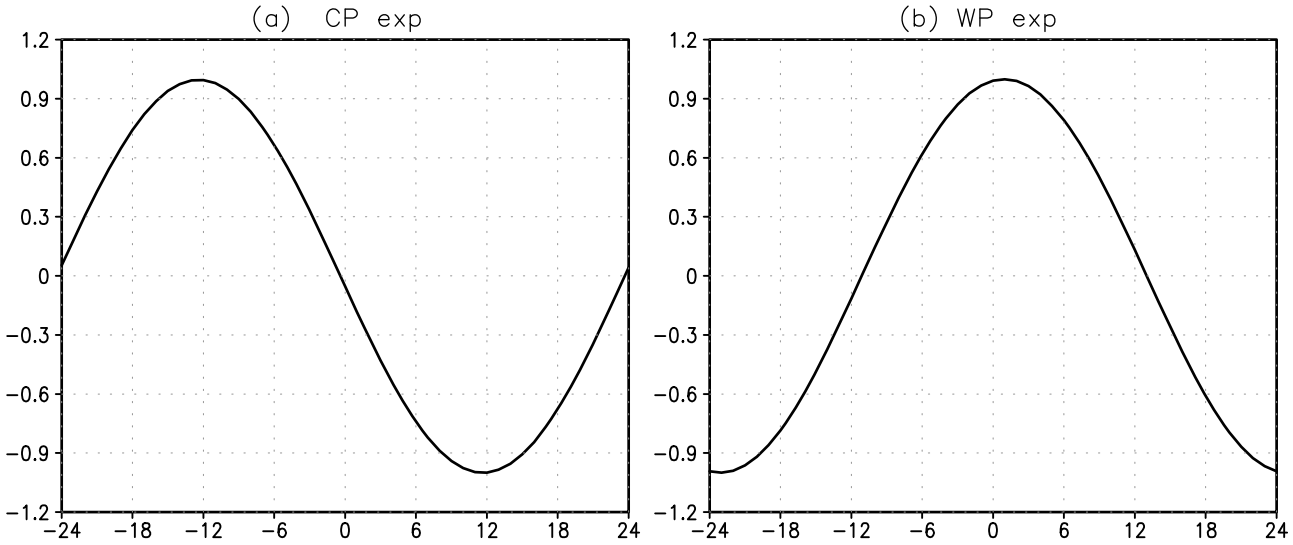

Figure 4. Lagged correlation between the wind stress forcing and the zonal mean thermocline (150°E–250°E, and 5°S–5°N) simulated from the CZ model in (a) CP Exp and (b) WP exp. See the text for experiment details. Unit on the horizontal axis is month.

WPU and the ZH. Therefore, the precursor signals of WP westerlies and positive zonal mean sea level can be understood as results of the same coupled process.

[21] Figure 2 (right) also shows a lead regression for each variable during NDJ with respect to the FMA WPU index. The regression pattern clearly shows the well-known pattern for the El Niño mature phase. The strong SST anomaly (Figure 2b) is located over the central to the eastern Pacific. Also, precipitation (Figure 2c) and zonal wind (Figure 2a) anomalies appear over the central Pacific. The HF (Figure 2d) variability becomes stronger near the dateline, but weaker over the far-western Pacific, consistent with the observation of *Kug et al.* [2008a]. The sea level anomaly (Figure 2e) shows an east-west contrast pattern. These patterns are similar to the linear regression map of the NDJ NINO3.4, indicating that the pattern is associated with El Niño peak phase.

3.4. Possible Interaction Between the Precursors

[22] So far, we have shown that the HF and LF precursors of El Niño/La Niña onset are highly correlated to each other. Such a high cross correlation implies that the precursors are mutually dependent and are part of the same coupled system. Based on the statistical relation, we suggest here a possible mechanism associated with the onset-related coupling process over the western Pacific. Firstly, there is a scale interaction scenario between LF wind and HF variability during the ENSO onset phase as follows. On the one hand, the LF westerlies give favorable conditions for stronger HF atmospheric variability through the change of the background vertical and horizontal shears over the equatorial western Pacific [*Seiki and Takayabu*, 2007b; *Kug et al.*, 2009a; *Sooraj et al.*, 2009]. On the other hand, due to the nonlinearity of the atmospheric precipitation (positive only) process, the HF westerly in the lower troposphere is

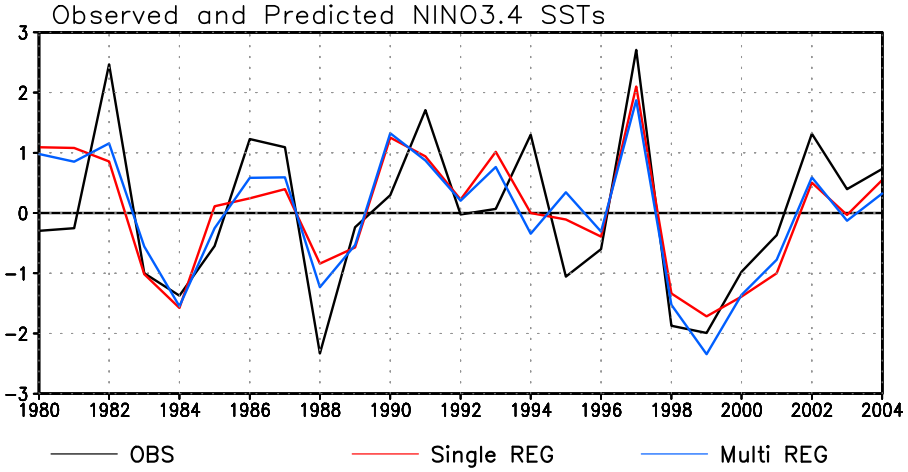

Figure 5. Observed (black line) and predicted NINO3.4 SST (NDJ) time series by single regression model (red line) and multiple regression model (blue line).

Table 2. Correlation Skill of Reconstructed NINO3.4 SST for Different Seasons[a]

	JFM	FMA	MAM
Composite index	0.69	0.76	0.80
Multiple index	0.75	0.80	0.82
Composite and multiple index	0.92	0.96	0.98
Composite index with cross validation	0.63	0.72	0.78
Multiple index with cross validation	0.66	0.70	0.75

[a]Composite index are made using HFU, WPU, and ZH. See the text for more details. JFM, January-February-March; FMA, February-March-April; MAM, March-April-May.

greatly enhanced through the convergence induced by heating while the HF easterly lacks such a circulation-convection feedback process. As a result, the HF zonal wind is highly positive skewed. It is possible that the asymmetric feature of the HF zonal wind modulates LF wind by the nonlinear rectification effect. This nonlinear rectification effect may reinforce the LF westerlies because the residual of the HF wind is proportional to the variance of the HF. If this process works from HF wind to LF wind, it is a two-way feedback process that enhances both the HF and LF wind components.

[23] The LF westerly wind over the western Pacific leads to SST increase and sea level (equatorial) rise over the western-central Pacific by inducing equatorial downwelling, thermocline deepening and eastward currents. The warm SST in turn alters precipitation and large-scale atmospheric circulation, enhancing the low-level westerlies over the western Pacific. As the western Pacific wind is not efficient in discharging the equatorial heat content compared to the central Pacific wind, this prolongs the positive feedback between the WPU, CPSST and ZH during the onset period. Throughout both the HF-LF and air-sea feedback processes, the precursor anomalies are gradually amplified, leading to the onset of El Niño and La Niña. However, although we showed distinctive correlation between the key variables, the coupling process should be further examined in a future study.

4. ENSO Prediction

[24] In section 3, we showed three onset precursors are closely coupled to each other. To support this argument further, we used the simplest statistical prediction model based on linear regression methods. First, a multiple linear regression model is developed and examined. In this case, the predictors are the three precursors during FMA and the predictand is NINO3.4 SST during NDJ. This is approximately a 9-month-lead forecast. In the multiple regression model, optimal weighing coefficients are calculated by a least square method. In this method, it is assumed that the predictors are independent. However, if the predictors are governed by the same process or they are strongly dependent, it is necessary to use just one predictor to represent their variability. Therefore, another predictor index is also defined by simply averaging the three normalized predictors. Using this predictor index (i.e., a composite index), a linear regression model is also developed and results are compared with those from the multiple linear regression model.

[25] Figure 5 shows the predicted NINO3.4 SST using both the multiple linear regression models and the single linear regression model without the cross validation. Two predicted SST time series capture the observed NINO3.4 SST evolution quite well. It is interesting that two predicted time series are consistent with each other, even when they failed to predict the observed values. For example, they both failed to predict the values observed in years 1980, 1981, 1990, 1993, and 1994, but they predict the same phase. The correlation skills are 0.80 for the multiple regressions and 0.76 for the single regression. Though the multiple regression is better than the single regression, the difference in correlation skills is not significant in spite of the non-cross-validation results.

[26] We also tested the predictions using the precursors of different seasons (e.g., JFM and MAM). These are approximately 10- and 8-month-lead forecasts. The prediction is carried out using these precursors and prediction skills are compared in Table 2. The correlation skill of the single linear regression is comparable with that of the multiple regression. The shorter the lead time, the smaller the difference is. Note that the correlations between two predicted time series are quite high (more than 0.9). In particular, when the precursors are based on MAM, the correlation is 0.98, indicating that they always have almost same prediction. This again indicates that the three precursors are not independent.

[27] The correlation skill mentioned above cannot be considered as an actual prediction skill, because the prediction model was developed using all data, including the data in the target year of prediction. To avoid this problem, the cross validation is carried out and the correlation skill is recalculated. In this case, the linear regression model is developed by excluding the data of the target year. As expected, the correlation skill is degraded as compared to the previous non-cross-validation skill. However, this method still shows a good correlation skill (see Table 2). For example, the correlation skill is more than 0.7, when the FMA data are used. It is comparable with the skill of the prediction in the state-of-the-art coupled GCMs [*Wang et al.*, 2008, 2009; *Jin et al.*, 2008] and the statistical multimodel ensemble [*Kug et al.*, 2007]. It is interesting to note that the skill of the multiple regression is more degraded, compared to that of the single regression. This is related to the so-called overfitting problem when a large number of predictors are used in a limited sample size (cf. *Kug et al.*, 2008b, 2008c]. As a result, the skill of the single regression is even better than that of the multiple regression, using the precursors in FMA and MAM seasons. These results suggest that the three precursors are governed by the same coupled process and the composite index is good enough to be used as a precursor of the ENSO onset.

5. Summary and Discussion

[28] In this study, cross relationship between the precursors of El Niño/La Niño onset is investigated. It is shown that three precursors are highly correlated to each other. In particular, the LF western Pacific zonal wind is closely related to the HF atmospheric variability such as MJO and WWE. In addition, a remarkable finding is that the western Pacific wind can induce a fast and efficient zonal mean

thermocline adjustment, which is dynamically different from the thermocline response to the central Pacific wind stress forcing, referred to the recharge process [*Jin*, 1996, 1997a, 1997b; *Li*, 1997]. Based on the observed strong correlation between the precursors, a possible two-way feedback process is hypothesized.

[29] Firstly, there is an internal atmospheric scale interaction between LF and HF wind variability over the western Pacific during the ENSO onset phase. The LF westerlies give favorable conditions for stronger HF variability through the change of the background vertical and horizontal shears [*Seiki and Takayabu*, 2007a, 2007b; *Kug et al.*, 2009a; *Sooraj et al.*, 2009]. In turn, the strong HF variability gives a positive feedback to the LF flow because of the highly skewed HF wind characteristics. This two-way feedback process enhances both the components. Secondly, there is a strong local air-sea coupling between the LF wind and SST. The western Pacific westerlies lead to the rise of the zonal mean equatorial sea level and increase the central Pacific SST through induced equatorial downwelling, deepening of thermocline and eastward currents, whose processes are similar to the new types of El Niño [*Kug et al.*, 2009b]. The warmer SST further amplifies the westerly through an enhanced precipitation and atmospheric heating. This air-sea coupling reinforces each component. The amplification of the HF and LF western Pacific wind and the equatorial heat content due to the aforementioned feedback processes eventually trigger the onset of El Niño and La Niña.

[30] In the previous ENSO paradigms, air-sea coupled processes over the central eastern Pacific are emphasized. The strong eastern Pacific warming weakens the equatorial trade wind over the central Pacific, which reinforces the warming again. This Bjerknes feedback has been well understood. However, our observational evidence supports that a strong coupling between HF and LF winds and between the ocean and atmosphere happens over the western Pacific prior to the ENSO onset. The current study extends the previous studies by *Weisberg and Wang* [1997a, 1997b] and *Kug et al.* [2005] who revealed only the LF zonal wind signal in the far western Pacific for ENSO onset and transition. The exact physical mechanism that gives rise to the connection between the HF and LF winds is still an open question, because our arguments are mostly based on the statistical relation. A detailed dynamical mechanism should be examined in further studies.

[31] **Acknowledgment.** This work was supported by the National Research Foundation of Korea Grant funded by the Korean Government (MEST) (NRF-2009-C1AAA001-2009-0093042).

References

An, S.-I. (2004), Interdecadal changes in El Niño–La Niña asymmetry, *Geophys. Res. Lett.*, *31*, L23210, doi:10.1029/2004GL021699.

An, S.-I., and I.-S. Kang (2000), A further investigation of the recharge oscillator paradigm for ENSO using a simple coupled model with the zonal mean and eddy separated, *J. Clim.*, *13*, 1987–1993, doi:10.1175/1520-0442(2000)013<1987:AFIOTR>2.0.CO;2.

An, S.-I., and B. Wang (2000), Interdecadal change of the structure of ENSO mode and its impact on the ENSO frequency, *J. Clim.*, *13*, 2044–2055, doi:10.1175/1520-0442(2000)013<2044:ICOTSO>2.0.CO;2.

An, S.-I., Y.-G. Ham, J.-S. Kug, F.-F. Jin, and I.-S. Kang (2005), El Niño–La Niña asymmetry in the Coupled Model Intercomparison Project simulations, *J. Clim.*, *18*, 2617–2627.

Barnston, A. G., M. H. Glantz, and Y. He (1999), Predictive skill of statistical and dynamical climate models in SST forecasts during the 1997–98 El Niño episode and the 1998 La Niña onset, *Bull. Am. Meteorol. Soc.*, *80*, 217–244, doi:10.1175/1520-0477(1999)080<0217:PSOSAD>2.0.CO;2.

Behringer, D. W., and Y. Xue (2004), Evaluation of the global ocean data assimilation system at NCEP: The Pacific Ocean, paper presented at Eighth Symposium on Integrated Observing and Assimilation Systems for Atmosphere, Oceans, and Land Surface, Am. Meteorol. Soc., Seattle, Wash.

Blanke, R., J. D. Neelin, and D. Gutzler (1997), Estimating the effect of stochastic wind stress forcing on ENSO irregularity, *J. Clim.*, *10*, 1473–1486, doi:10.1175/1520-0442(1997)010<1473:ETEOSW>2.0.CO;2.

Cassou, C., and C. Perigaud (2000), ENSO simulated by intermediate coupled models and evaluated with observations over 1970–98. Part II: Role of the off-equatorial ocean and meridional winds, *J. Clim.*, *13*, 1635–1663, doi:10.1175/1520-0442(2000)013<1635:ESBICM>2.0.CO;2.

Chang, P., L. Zhang, R. Saravanan, D. J. Vimont, J. C. H. Chiang, L. Ji, H. Seidel, and M. K. Tippett (2007), Pacific meridional mode and El Niño—Southern Oscillation, *Geophys. Res. Lett.*, *34*, L16608, doi:10.1029/2007GL030302.

Chiang, J. C. H., and D. J. Vimont (2004), Analogous Pacific and Atlantic meridional modes of tropical atmosphere-ocean variability, *J. Clim.*, *17*, 4143–4158, doi:10.1175/JCLI4953.1.

Clarke, A. J., and S. Van Gorder (2003), Improving El Niño prediction using a space-time integration of Indo-Pacific winds and equatorial Pacific upper ocean heat content, *Geophys. Res. Lett.*, *30*(7), 1399, doi:10.1029/2002GL016673.

Curtis, S., R. F. Adler, G. J. Huffman, and G. Gu (2004), Westerly wind events and precipitation in the eastern Indian Ocean as predictors for El Niño: Climatology and case study for the 2002–2003 El Niño, *J. Geophys. Res.*, *109*, D20104, doi:10.1029/2004JD004663.

Duchon, C. (1979), Lancos filtering in one and two dimensions, *J. Appl. Meteorol.*, *18*, 1016–1022, doi:10.1175/1520-0450(1979)018<1016:LFIOAT>2.0.CO;2.

Eisenman, I., L. Yu, and E. Tziperman (2005), Westerly wind bursts: ENSO's tail rather than the dog?, *J. Clim.*, *18*, 5224–5238, doi:10.1175/JCLI3588.1.

Hendon, H. H., M. Wheeler, and C. Zhang (2007), Seasonal dependence of the MJO-ENSO relationship, *J. Clim.*, *20*, 531–543, doi:10.1175/JCLI4003.1.

Ji, M., R. W. Reynolds, and D. W. Behringer (2000), Use of TOPEX/Poseidon sea level data for ocean analyses and ENSO prediction: Some early results, *J. Clim.*, *13*, 216–231, doi:10.1175/1520-0442(2000)013<0216:UOTPSL>2.0.CO;2.

Jin, E. K., et al. (2008), Current status of ENSO prediction skill in coupled ocean-atmosphere models, *Clim. Dyn.*, *31*, doi:10.1007/s00382-008-0397-3.

Jin, F.-F. (1996), Tropical ocean-atmosphere interaction, the Pacific cold tongue, and the El Niño–Southern Oscillation, *Science*, *274*, 76–78, doi:10.1126/science.274.5284.76.

Jin, F.-F. (1997a), An equatorial ocean recharge paradigm for ENSO. Part I: conceptual model, *J. Atmos. Sci.*, *54*, 811–829, doi:10.1175/1520-0469(1997)054<0811:AEORPF>2.0.CO;2.

Jin, F.-F. (1997b), An equatorial ocean recharge paradigm for ENSO. Part II: A stripped-down coupled model, *J. Atmos. Sci.*, *54*, 830–847, doi:10.1175/1520-0469(1997)054<0830:AEORPF>2.0.CO;2.

Kalnay, E., et al. (1996), The NCEP/NCAR 40-year reanalysis project, *Bull. Am. Meteorol. Soc.*, *77*, 437–471, doi:10.1175/1520-0477(1996)077<0437:TNYRP>2.0.CO;2.

Kang, I.-S., and J.-S. Kug (2000), An El Niño prediction system with an intermediate ocean and statistical atmosphere model, *Geophys. Res. Lett.*, *27*, 1167–1170, doi:10.1029/1999GL011023.

Kang, I.-S., and J.-S. Kug (2002), El Niño and La Niña sea surface temperature anomalies: Asymmetry characteristics associated with their wind stress anomalies, *J. Geophys. Res.*, *107*(D19), 4372, doi:10.1029/2001JD000393.

Kessler, W. S. (2002), ENSO a cycle or a series of events?, *Geophys. Res. Lett.*, *29*(23), 2125, doi:10.1029/2002GL015924.

Kessler, W. S., and M. J. McPhaden (1995), Oceanic equatorial waves and the 1991–93 El Niño, *J. Clim.*, *8*, 1757–1774, doi:10.1175/1520-0442(1995)008<1757:OEWATE>2.0.CO;2.

Kug, J.-S., and I.-S. Kang (2006), Interactive feedback between the Indian Ocean and ENSO, *J. Clim.*, *19*, 1784–1801.

Kug, J.-S., I.-S. Kang, and S.-I. An (2003), Symmetric and antisymmetric mass exchanges between the equatorial and off-equatorial Pacific associated with ENSO, *J. Geophys. Res.*, *108*(C8), 3284, doi:10.1029/2002JC001671.

Kug, J.-S., S.-I. An, F.-F. Jin, and I.-S. Kang (2005), Preconditions for El Niño and La Niña onsets and their relation to the Indian Ocean, *Geophys. Res. Lett.*, *32*, L05706, doi:10.1029/2004GL021674.

Kug, J.-S., B. P. Kirtman, and I.-S. Kang (2006a), Interactive feedback between ENSO and the Indian Ocean in an interactive coupled model, *J. Clim.*, *19*, 6371–6381.

Kug, J.-S., T. Li, S.-I. An, I.-S. Kang, J.-J. Luo, S. Masson, and T. Yamagata (2006b), Role of the ENSO-Indian Ocean coupling on ENSO variability in a coupled GCM, *Geophys. Res. Lett.*, *33*, L09710, doi:10.1029/2005GL024916.

Kug, J.-S., J.-Y. Lee, and I.-S. Kang (2007), Global sea surface temperature prediction using a multi-model ensemble, *Mon. Weather Rev.*, *135*, 3239–3247, doi:10.1175/MWR3458.1.

Kug, J.-S., F.-F. Jin, K. P. Sooraj, and I.-S. Kang (2008a), State-dependent atmospheric noise associated with ENSO, *Geophys. Res. Lett.*, *35*, L05701, doi:10.1029/2007GL032017.

Kug, J.-S., J.-Y. Lee, and I.-S. Kang (2008b), Systematic bias correction of dynamical seasonal prediction with a stepwise pattern projection method (SPPM), *Mon. Weather Rev.*, *136*, 3501–3512, doi:10.1175/2008MWR2272.1.

Kug, J.-S., J.-Y. Lee, and I.-S. Kang (2008c), Optimal multi-model ensemble method in seasonal climate prediction: Asia-Pacific, *J. Atmos. Sci.*, *44*, 259–267.

Kug, J.-S., K. P. Sooraj, D. Kim, I.-S. Kang, F.-F. Jin, Y. N. Takayabu, and M. Kimoto (2009a), Simulation of state-dependent high frequency atmospheric variability associated with ENSO, *Clim. Dyn.*, *32*, 635–648, doi:10.1007/s00382-008-0434-2.

Kug, J.-S., F.-F. Jin, and S.-I. An (2009b), Two types of El Niño events: Cold tongue El Niño and warm pool El Niño, *J. Clim.*, *22*, 1499–1515, doi:10.1175/2008JCLI2624.1.

Li, T. (1997), Phase transition of the El Niño–Southern Oscillation: A stationary SST mode, *J. Atmos. Sci.*, *54*, 2872–2887, doi:10.1175/1520-0469(1997)054<2872:PTOTEN>2.0.CO;2.

Luo, J. J., S. Masson, S. K. Behera, and T. Yamagata (2008), Extended ENSO predictions using a fully coupled ocean–atmosphere model, *J. Clim.*, *21*, 84–93, doi:10.1175/2007JCLI1412.1.

McPhaden, M. J. (1999), Genesis and evolution of the 1997–98 El Niño, *Science*, *283*, 950–954, doi:10.1126/science.283.5404.950.

Meinen, C. S., and M. J. McPhaden (2000), Observations of warm water volume changes in the equatorial Pacific and their relationship to El Niño and La Niña, *J. Clim.*, *13*, 3551–3559, doi:10.1175/1520-0442(2000)013<3551:OOWWVC>2.0.CO;2.

Meinen, C. S., and M. J. McPhaden (2001), Interannual variability in warm water volume transports in the equatorial Pacific during 1993–99, *J. Phys. Oceanogr.*, *31*, 1324–1345, doi:10.1175/1520-0485(2001)031<1324:IVIWWV>2.0.CO;2.

Perigaud, C., F. Melin, and C. Cassou (2000), ENSO simulated by intermediate models and evaluated with observations over 1970–98. Part I: Role of the off-equatorial variability, *J. Clim.*, *13*, 1605–1634, doi:10.1175/1520-0442(2000)013<1605:ESBICM>2.0.CO;2.

Rodgers, K. B., P. Friederichs, and M. Latif (2004), Tropical Pacific decadal variability and its relation to decadal modulations of ENSO, *J. Clim.*, *17*, 3761–3774, doi:10.1175/1520-0442(2004)017<3761:TPDVAI>2.0.CO;2.

Seiki, A., and Y. N. Takayabu (2007a), Westerly wind bursts and their relationship with intraseasonal variations and ENSO. Part I: Statistics, *Mon. Weather Rev.*, *135*, 3325–3345, doi:10.1175/MWR3477.1.

Seiki, A., and Y. N. Takayabu (2007b), Westerly wind bursts and their relationship with intraseasonal variations and ENSO, Part II: Energetics over the western and central Pacific, *Mon. Weather Rev.*, *135*, 3346–3361, doi:10.1175/MWR3503.1.

Smith, T. M., and R. W. Reynolds (2004), Improved extended reconstruction of SST (1854–1997), *J. Clim.*, *17*, 2466–2477, doi:10.1175/1520-0442(2004)017<2466:IEROS>2.0.CO;2.

Sooraj, K. P., D. Kim, J.-S. Kug, S.-W. Yeh, F.-F. Jin, and I.-S. Kang (2009), Effects of the low frequency zonal wind variation on the high-frequency atmospheric variability over the tropics, *Clim. Dyn.*, *33*, 495–507, doi:10.1007/s00382-008-0483-6.

Tang, Y., and B. Yu (2008), MJO and its relationship to ENSO, *J. Geophys. Res.*, *113*, D14106, doi:10.1029/2007JD009230.

Vimont, D. J., D. S. Battisti, and A. C. Hirst (2001), Footprinting: A seasonal connection between the tropics and mid-latitudes, *Geophys. Res. Lett.*, *28*, 3923–3926, doi:10.1029/2001GL013435.

Vimont, D. J., J. M. Wallace, and D. S. Battisti (2003a), The seasonal footprinting mechanism in the Pacific: Implications for ENSO, *J. Clim.*, *16*, 2668–2675, doi:10.1175/1520-0442(2003)016<2668:TSFMIT>2.0.CO;2.

Vimont, D. J., D. S. Battisti, and A. C. Hirst (2003b), The seasonal footprinting mechanism in the CSIRO general circulation models, *J. Clim.*, *16*, 2653–2667, doi:10.1175/1520-0442(2003)016<2653:TSFMIT>2.0.CO;2.

Wang, B., and X. Xie (1996), Low-frequency equatorial waves in vertically sheared zonal flow. Part I: Stable waves, *J. Atmos. Sci.*, *53*, 449–467, doi:10.1175/1520-0469(1996)053<0449:LFEWIV>2.0.CO;2.

Wang, B., R. Wu, and X. Fu (2000), Pacific–East Asia teleconnection: How does ENSO affect East Asian climate?, *J. Clim.*, *13*, 1517–1536, doi:10.1175/1520-0442(2000)013<1517:PEATHD>2.0.CO;2.

Wang, B., R. Wu, R. Lukas, and S. I. An (2001), A possible mechanism for ENSO turnabout, in *Dynamics of Atmospheric General Circulation and Climate*, pp. 552–578, China Meteorol. Press, Beijing.

Wang, B., J.-Y. Lee, I.-S. Kang, J. Shukla, J.-S. Kug, A. Kumar, J. Schemm, J.-J. Luo, T. Yamagata, and C.-K. Park (2008), How accurately do coupled models predict the Asian-Australian Monsoon interannual variability?, *Clim. Dyn.*, *30*, 605–619, doi:10.1007/s00382-007-0310-5.

Wang, B., et al. (2009), Advance and prospectus of seasonal prediction: assessment of the APCC/CliPAS 14-model ensemble retrospective seasonal prediction (1980–2004), *Clim. Dyn.*, *33*, 93–117, doi:10.1007/s00382-008-0460-0.

Watanabe, M., and F.-F. Jin (2003), A moist linear baroclinic model: Coupled dynamical–convective response to El Niño, *J. Clim.*, *16*, 1121–1140, doi:10.1175/1520-0442(2003)16<1121:AMLBMC>2.0.CO;2.

Weisberg, R. H., and C. Wang (1997a), A western Pacific oscillator paradigm for the El Niño–Southern Oscillation, *Geophys. Res. Lett.*, *24*, 779–782, doi:10.1029/97GL00689.

Weisberg, R. H., and C. Wang (1997b), Slow variability in the equatorial west- central Pacific in relation to ENSO, *J. Clim.*, *10*, 1998–2002, doi:10.1175/1520-0442(1997)010<1998:SVITEW>2.0.CO;2.

Xie, P., and P. A. Arkin (1997), Global precipitation: A 17-year monthly analysis based on gauge observations, satellite estimates, and numerical model outputs, *Bull. Am. Meteorol. Soc.*, *78*, 2539–2558, doi:10.1175/1520-0477(1997)078<2539:GPAYMA>2.0.CO;2.

Xie, S.-P., K. Hu, J. Hafner, H. Tokinaga, Y. Du, G. Huang, and T. Sampe (2009), Indian Ocean capacitor effect on Indo-western Pacific climate during the summer following El Niño, *J. Clim.*, *22*, 730–747, doi:10.1175/2008JCLI2544.1.

Yu, J.-Y., and C. R. Mechoso (2001), Coupled atmosphere–ocean GCM study of the ENSO cycle, *J. Clim.*, *14*, 2329–2350, doi:10.1175/1520-0442(2001)014<2329:ACAOGS>2.0.CO;2.

Zebiak, S. E., and M. Cane (1987), A model El Niño–Southern Oscillation, *Mon. Weather Rev.*, *115*, 2262–2278, doi:10.1175/1520-0493(1987)115<2262:AMENO>2.0.CO;2.

F.-F. Jin, Department of Meteorology, SOEST, University of Hawai'i at Mānoa, 1680 East-West Rd., Honolulu, HI 96822, USA. (jff@hawaii.edu)

J.-S. Kug, Korea Ocean Research and Development Institute, 1270 Sang-rok gu, Ansan-Si, KyungKi-Do, Ansan, Korea. (jskug@kordi.re.kr)

T. Li and K.-P. Sooraj, International Pacific Research Center, SOEST, University of Hawai'i at Mānoa, 1680 East-West Rd., Honolulu, HI 96822, USA. (timli@hawaii.edu; soorajmet@gmail.com)